Cellular/Molecular

The Lactate Receptor HCAR1 Modulates Neuronal Network Activity through the Activation of G_{α} and $G_{\beta\gamma}$ Subunits

Haíssa de Castro Abrantes,[1] Marc Briquet,[1] Céline Schmuziger,[1] Leonardo Restivo,[1] Julien Puyal,[1] Nadia Rosenberg,[1] Anne-Bérengère Rocher,[1] Stefan Offermanns,[3] and Jean-Yves Chatton[1,2]

[1]Department of Fundamental Neuroscience, [2]Cellular Imaging Facility, University of Lausanne, 1005 Lausanne, Switzerland, and [3]Department of Pharmacology, Max-Planck-Institute for Heart and Lung Research, 61231 Bad Nauheim, Germany

The discovery of a G-protein-coupled receptor for lactate named hydroxycarboxylic acid receptor 1 (HCAR1) in neurons has pointed to additional nonmetabolic effects of lactate for regulating neuronal network activity. In this study, we characterized the intracellular pathways engaged by HCAR1 activation, using mouse primary cortical neurons from wild-type (WT) and HCAR1 knock-out (KO) mice from both sexes. Using whole-cell patch clamp, we found that the activation of HCAR1 with 3-chloro-5-hydroxybenzoic acid (3Cl-HBA) decreased miniature EPSC frequency, increased paired-pulse ratio, decreased firing frequency, and modulated membrane intrinsic properties. Using fast calcium imaging, we show that HCAR1 agonists 3,5-dihydroxybenzoic acid, 3Cl-HBA, and lactate decreased by 40% spontaneous calcium spiking activity of primary cortical neurons from WT but not from HCAR1 KO mice. Notably, in neurons lacking HCAR1, the basal activity was increased compared with WT. HCAR1 mediates its effect in neurons through a $G_{i\alpha}$-protein. We observed that the adenylyl cyclase– cAMP–protein kinase A axis is involved in HCAR1 downmodulation of neuronal activity. We found that HCAR1 interacts with adenosine A1, $GABA_B$, and α_{2A}-adrenergic receptors, through a mechanism involving both its $G_{i\alpha}$ and $G_{i\beta\gamma}$ subunits, resulting in a complex modulation of neuronal network activity. We conclude that HCAR1 activation in neurons causes a downmodulation of neuronal activity through presynaptic mechanisms and by reducing neuronal excitability. HCAR1 activation engages both $G_{i\alpha}$ and $G_{i\beta\gamma}$ intracellular pathways to functionally interact with other G_i-coupled receptors for the fine tuning of neuronal activity.

Key words: GPR81; HCAR1; intracellular pathway; lactate; neurons; spontaneous activity

Significance Statement

Expression of the lactate receptor hydroxycarboxylic acid receptor 1 (HCAR1) was recently described in neurons. Here, we describe the physiological role of this G-protein-coupled receptor (GPCR) and its activation in neurons, providing information on its expression and mechanism of action. We dissected out the intracellular pathway through which HCAR1 activation tunes down neuronal network activity. For the first time, we provide evidence for the functional cross talk of HCAR1 with other GPCRs, such as $GABA_B$, adenosine A1- and α_{2A}-adrenergic receptors. These results set HCAR1 as a new player for the regulation of neuronal network activity acting in concert with other established receptors. Thus, HCAR1 represents a novel therapeutic target for pathologies characterized by network hyperexcitability dysfunction, such as epilepsy.

Introduction

Lactate has long been considered a waste product of cellular metabolism. In the CNS, this concept was challenged in the 1990s when lactate was proposed to play an important role as energy substrate for neurons (Pellerin and Magistretti, 1994). Since then, several studies indicated the valuable contribution of lactate as a metabolic fuel in several cell types, as a neuroprotective agent, as well as its role as a signaling molecule (for review, see Gladden, 2004; Barros, 2013).

The extracellular level of lactate in the brain is estimated to be in the low-millimolar range at the resting state (Abi-Saab et al., 2002). It has also been reported that physical exercise increases L-lactate plasma levels up to 10–20 mM (Offermanns, 2017). Under these conditions, the brain becomes a net consumer of lactate (Dalsgaard et al., 2004). Upon synaptic activity, lactate level undergoes a twofold increase (Dienel et al., 2007). The main cell type locally producing lactate in the brain is likely to be astrocytes, as recently reported in the *in vivo* mouse brain (Mächler et al., 2016), although this notion was recently challenged (Díaz-García

Received Aug. 10, 2018; revised March 19, 2019; accepted March 22, 2019.

Author contributions: H.d.C.A., L.R., N.R., A.-B.R., and J.-Y.C. designed research; H.d.C.A., M.B., C.S., J.P., A.-B.R., and J.-Y.C. performed research; S.O. contributed unpublished reagents/analytic tools; H.d.C.A., M.B., C.S., L.R., J.P., A.-B.R., and J.-Y.C. analyzed data; H.d.C.A. and J.-Y.C. wrote the paper

This work was supported by the Swiss National Science Foundation (Grant #31003A_179399). The Epac2-camps plasmid was provided by Jean-Pierre Hornung (University of Lausanne, Lausanne, Switzerland). We thank Joel Wellbourne-Wood for critical reading of the manuscript and Christiane Devenoges for the genotyping.

The authors declare no competing financial interests.

Correspondence should be addressed to Jean-Yves Chatton at jean-yves.chatton@unil.ch.

https://doi.org/10.1523/JNEUROSCI.2092-18.2019

et al., 2017). The recent discovery of a new mechanism for lactate release from astrocytes through a K^+-sensitive channel (Sotelo-Hitschfeld et al., 2015) indicates that lactate can be rapidly mobilized and may possibly lead to a transient elevation of its extracellular concentration to high levels in microdomains close to neuronal membranes, including synapses.

Recent studies indicated that energy substrates and metabolites of the energy metabolism had extracellular signaling properties by acting through the activation of G-protein-coupled receptors (GPCRs; Blad et al., 2012; Husted et al., 2017). One of them, originally named GPR81, now known as hydroxycarboxylic acid receptor 1 (HCAR1), has lactate as an endogenous ligand (Cai et al., 2008). HCAR1 was initially described as being markedly expressed in adipocytes, where its activation induces the inhibition of lipolysis through the activation of a G_i-dependent intracellular pathway (Liu et al., 2009). Our research group was the first to demonstrate that L-lactate and a HCAR1 agonist decreases spiking activity of cortical neurons in a pertussis-sensitive manner (Bozzo et al., 2013). In the locus ceruleus, L-lactate had rather an excitatory effect, suggesting the involvement of a different receptor, possibly G_s coupled, yet to be identified (Tang et al., 2014). The aim of the present study was to explore the downstream effectors of HCAR1 activation and clarify the mechanisms through which this receptor modulates neuronal activity in mouse cortical neurons.

We focused on the investigation of the intracellular pathway mediated by the activation of G_i-coupled receptors, which classically inhibits the adenylyl cyclase (AC) as a first phase of the intracellular cascade that contributes to the decrease in neuronal activity (Seino and Shibasaki, 2005). To explore these aspects, we compared the modulatory effects of HCAR1 activation on neuronal activity of primary neurons from both wild-type (WT) and HCAR1 knock-out (KO) mice, using electrophysiological recordings and calcium imaging. Our study indicates that HCAR1 activation engages the AC–cAMP–protein kinase A (PKA) pathway and has a presynaptic effect, which is accompanied by a decrease in neuronal excitability. We further discovered that HCAR1 interacts with other G_i-coupled receptors to fine-tune neuronal activity through a complex bimodal mechanism that involves the $G_{\beta\gamma}$ subunit and activation of phospholipase C (PLC). This interaction adds a higher level of complexity to the functional outcome of HCAR1 activation.

Materials and Methods

Ethics statement. All experimental procedures were performed in accordance with the recommendations of the Swiss Ordinance on Animal Experimentation and were specifically approved for this study by the Veterinary Affair of the Canton Vaud, Switzerland (authorizations #1288.6 and #1288.7).

Animals. HCAR1 KO and monomeric red fluorescent protein (mRFP)-HCAR1 mouse lines where obtained from Max-Planck-Institute for Heart and Lung Research (Bad Nauheim, Germany). The generation and validation of these lines have been previously described (Ahmed et al., 2010). The genotype of all animals used for the experiments was confirmed using PCR analysis.

Behavioral analysis. The assessment of general behavior along with neurological and motor functions was performed in WT and HCAR1 KO male mice (8 and 15 weeks). In a first phase, mice went through a basic neurological screening to assess their general behavior/appearance, muscle tone, and motor function. Mice were placed in a transparent Plexiglas box and observed for 5 min by an experimenter blind to the genotype of the animals. Mice were checked for stereotyped behavior, convulsions, compulsive licking, self-destructive biting, and retropulsion. Next, the grasping reflex was tested by suspending the mouse by the tail and giving a Yes/No score for hindpaw clasping over three consecutive trials. The grip strength was assessed by placing the animal on a grid and gently pulling its tail; the mean score of three trials per animal was used for analysis. In the second phase, home-cage behavior was monitored in PhenoTyper cages (Noldus; RRID:SCR_004074) that allow the automated scoring of parameters related to locomotion, stereotypic behavior, feeding, and nesting. Briefly, mice were individually placed inside the PhenoTyper cage for 1 d with water and food *ad libitum*. A shelter was placed in one corner of the cage for automated scoring of nesting behavior. An infrared camera tracked the mouse movements throughout the 1 d session, allowing the monitoring of the above parameters. All the behavior data were collected and analyzed using EthoVision XT 14 software (Noldus; RRID:SCR_000441).

Cell culture and transfection. Mouse primary cultures from cortical neurons were prepared from embryonic day 17 (E17) embryos, both male and female, from WT, HCAR1 KO, or mRFP-HCAR1 C57BL/6N mouse lines. After removing the meninges, extracted cortices were incubated in 2 ml of HBSS with 10 mg/ml Trypsin (Worthington Biochemical) for 20 min at 37°C, and then mechanically dissociated in Neurobasal culture medium (Invitrogen) supplemented with 10% FCS. Dissociated cells were filtered using a 40 μm nylon mesh cell strainer and resuspended in Neurobasal culture medium complemented with 2% SM1 (STEMCELL Technologies), 20 mM GlutaMAX (Invitrogen), and 0.02 mM glutamate. Cells were plated at a density of 20,000 cells/cm^2 in 12- and 20-mm-diameter glass coverslips, coated with poly-D-lysine and laminin (Sigma-Aldrich). Half of the culture medium was exchanged every 5 d by a maturation medium composed of BrainPhys medium (STEMCELL Technologies) and 2% SM1. Cells were used at day *in vitro* (DIV) 12–18.

Transfection with the plasmid carrying the cAMP fluorescent resonance energy transfer (FRET)-based biosensor (Epac2-camps; Nikolaev et al., 2004) was performed using Lipofectamine 2000 (Invitrogen) by adding 3 μg of DNA for 5–6 h. Cells were transfected at DIV 10–12 and used 48 h after transfection.

DNA extraction and PCR. Tissue was collected from phalanges of WT and HCAR1 KO E17 embryos used for the primary culture preparation. The tissue was incubated in the digestion buffer as follows (in mM): NaCl 100, Tris 10, EDTA 25, 0.5% SDS, and 5% Proteinase K (Roche), for 2 h at 57°C. After three steps of centrifugation, the pellet was dried out and resuspended in TE (Tris and EDTA) buffer (Tris-HCl, 10 mM, pH 7.5; EDTA, 0.1 mM). The DNA was amplified using the T-Personal Thermocycler (Biometra). The following two sets of primers were used to amplify the targets sequences: HCAR1: forward, TTCTGCTTTCACATG AAGACC; reverse, CAGAACAAGATGATTGTCAGG; and Neomycin: forward, GCAGCGCATCGCCTTCTATC; reverse, GATATCAGGTG GACAAGTCC.

Quantitative RT-PCR. Brains from WT ($n = 3$) and HCAR1 KO ($n = 3$) mice (1 month old) were dissected in 1 mM $MgCl_2$ RNase-free PBS, then frozen in liquid nitrogen, and kept at −80°C until use. RNA extraction from tissue or cultured neurons was performed using the commercial RNeasy Mini Kit (Qiagen), and 1 μg/μl was used for reverse transcription to cDNA with the High capacity cDNA Reverse Transcription Kit (Applied Biosystems). The cDNA was amplified by quantitative RT-PCR (qRT-PCR) using the Power SYBR Green PCR Master Mix (Bio-Rad), with specific primers for the target genes at 200 nM (HCAR1: GGGGACTGTGTATCTTCTGA, GAGTCTTGGTGTAGAATTTGG; GAPDH: TCCATGACAACTTTGGCATTG, CAGTCTTCTGGGTGG CAGTGA). Samples were run in triplicate, and negative controls were run for each target gene. All reactions were performed on a CFX96 Touch Real-Time PCR Detection System (Bio-Rad). Relative mRNA expression was quantified by using the comparative CT method, and results are shown as the fold change using the 2CT formula (Livak and Schmittgen, 2001).

Immunohistochemistry. Primary cortical neurons from mRFP-HCAR1 mice ($n = 2$) grown on coverslips were fixed with 4% paraformaldehyde in PBS for 15 min on ice. Cells were preincubated with 15% serum and 0.05% Triton X-100 and subsequently incubated overnight with the primary mouse anti-NeuN antibody (1:200; catalog #MAB377, EMD Millipore) and rabbit anti-mRFP (1:100; catalog #600–401-379, Rockland Immunochemicals). Cells were incubated with the appropriate secondary antibodies (i.e., 1:200; Alexa Fluor 488-conjugated donkey anti-

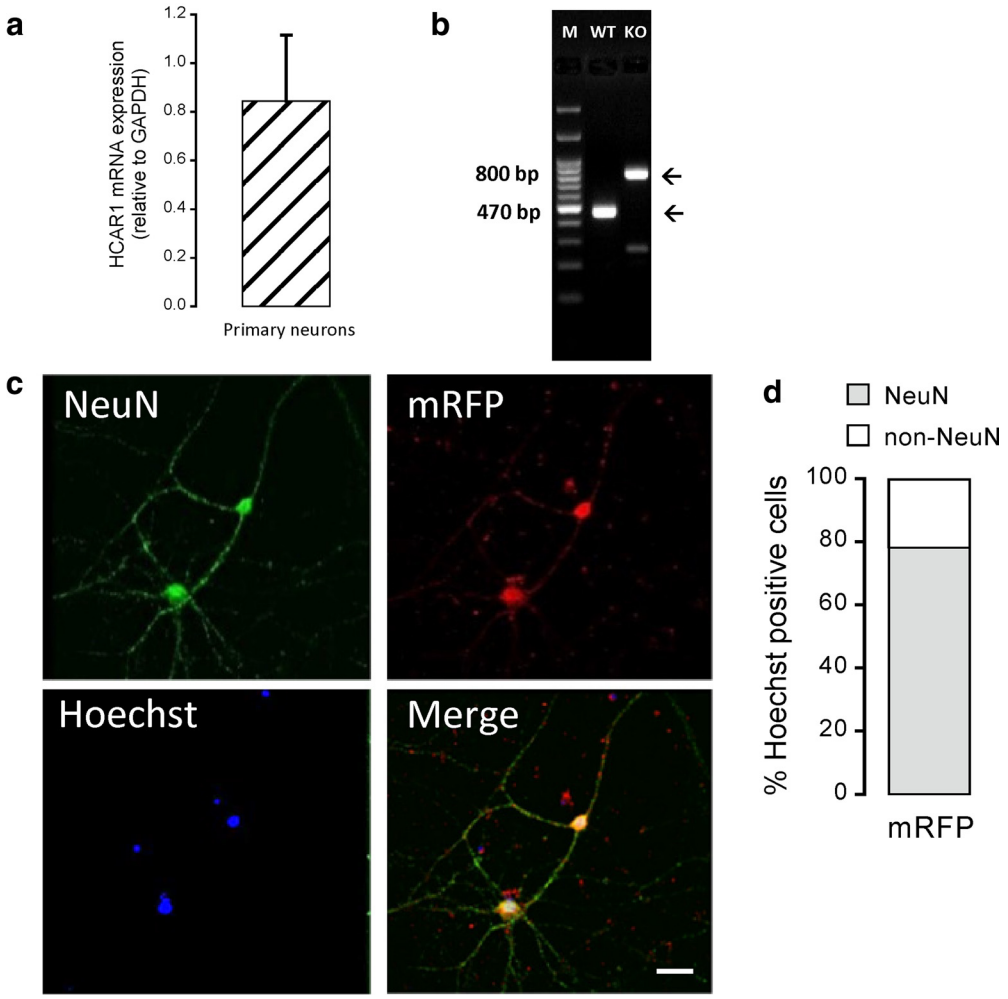

Figure 1. HCAR1 expression in primary mouse neurons. ***a***, HCAR1 mRNA expression level in primary neurons ($n = 4$ experiments). HCAR1 mRNA transcript levels were normalized relative to that of the housekeeping gene GAPDH. ***b***, Representative PCR image of HCAR1 gene expression in WT versus HCAR1 KO animals. WT and HCAR1 KO embryonic tissue were obtained from animals used to originate neuronal primary cultures. A WT band at 470 bp and a HCAR1 KO band at 800 bp can be observed. ***c***, Representative confocal images of primary cortical neurons immunostained for NeuN (green) and mRFP-HCAR1 (red), along with Hoechst nuclear staining (blue) and the overlay image. ***d***, Quantification of mRFP-, NeuN-, and mRFP-NeuN-positive cells shown as the percentage of Hoechst-positive cells ($n = 5$ experiments, repeated 3 times per experiment). Scale bar, 40 μm.

mouse IgG; catalog #ab105105, Abcam) and Alexa Fluor 594-conjugated donkey anti-rabbit IgG (1:200; catalog #ab150076, Abcam). Brain sections from 1-month-old WT ($n = 6$) and HCAR1 KO ($n = 5$) mice were obtained from mice anesthetized with sodium-pentobarbital (150 mg/kg, i.p.) and transcardially perfused with 4% paraformaldehyde. The brains were sliced in a sagittal or coronal plane using a vibratome (VT1000S, Leica), or were cryoprotected in 30% sucrose and sliced using a microtome (HM 400, Microm); in both cases, 30-μm-thick slices were obtained. Slices were preincubated with 15% donkey serum and 0.3% Triton X-100 and subsequently were incubated with the primary antibody overnight (Table 1-1, available at https://doi.org/10.1523/JNEUROSCI.2092-18.2019.t1-1). In sequence, slices were incubated with the appropriate secondary antibody (Table 1-2, available at https://doi.org/10.1523/JNEUROSCI.2092-18.2019.t1-2).

Nuclei were stained using Hoechst stain (Invitrogen). Negative controls were performed in the absence of primary antibodies. Coverslips and slices were mounted in FluorSave Mounting Medium (EMD Millipore). Coverslips were analyzed using the Leica TCS SP5 Confocal Microscope (Leica). Brain sections were analyzed using the Zeiss LSM 710 Confocal Microscope (Zeiss).

Western blot. Western blot was performed as previously described (Grishchuk et al., 2011), using WT ($n = 4$) and HCAR1 KO ($n = 4$) cortex, hippocampus, and cerebellum. Briefly, the different brain regions were dissected and then stored at −20°C in lysis buffer, containing the following (in mM): HEPES 20, pH 7.4, NaCl 10, $MgCl_2$ 3, EGTA 2.5, dithiothreitol 0.1, NaF 50, Na_3VO_4 1, 1% Triton X-100, and a protease inhibitor cocktail (catalog #1187350001, Roche). Protein concentration was determined using a Bradford assay. Proteins (30–40 μg) were separated on 12% polyacrylamide gels and analyzed by immunoblotting. Primary antibodies (Table 1-1, available at https://doi.org/10.1523/JNEUROSCI.2092-18.2019.t1-1) were diluted in blocking buffer with 0.001% PBS Tween-20 and incubated overnight at 4°C. Secondary antibodies (Table 1-2, available at https://doi.org/10.1523/JNEUROSCI.2092-18.2019.t1-2) were diluted in blocking buffer and incubated for 1 h. Protein bands were visualized with the Odyssey Infrared Imaging System (LI-COR) or by using the enhanced chemiluminescence (ECL) method, using 200 μl of ECL substrate (SuperSignal West Dura Extended Duration Substrate, Thermo Fisher Scientific). Odyssey version 1.2 software (LI-COR) or LAS 4000 Mini Luminescent Image Analyzer (FujiFilm) were used for analysis. Values were normalized with respect to actin.

Live-cell microscopy. Intracellular calcium imaging was performed on an upright epifluorescence microscope (model FN1, Nikon) using a 40×, 0.8 numerical aperture (NA), water-immersion objective lens. Fluorescence excitation wavelengths were selected using a fast filter wheel (Sutter Instrument) and fluorescence was detected using an Evolve Electron Multiplying CCD (EMCCD) Camera (Photometrics). Digital image acquisition and time series were computer controlled using MetaFluor software (Molecular Devices; RRID:SCR_014294). Up to eight individ-

Table 1. Anti-HCAR1 primary antibody specificity

Anti-HCAR1 primary antibody (source, reference)	Epitope	IHC		WB	
		WT	HCAR1 KO	WT	HCAR1 KO
Santa Cruz Biotechnology, SC-32647	C-terminal, extracellular domain of human HCAR1	§	§	+	+
Santa Cruz Biotechnology, SC-32648	C-terminal, cytoplasmic domain of human HCAR1	+	+	−	−
Sigma-Aldrich, SAB1300090	Mouse GPR81-S296, aa 276–329	+	+	+	+
Sigma-Aldrich, SAB1300793	Rat GPR81-R320, aa 286–332	+	+	§	§
Sigma-Aldrich, SAB1300089	Human GPR81–296, aa 310–353	+	+	+	+
Sigma-Aldrich, SAB1300792	Mouse GPR81-R203, aa 193–230	+	+	§	§
Sigma-Aldrich, SAB1300791	Mouse GPR81-C7, aa 7–36	+	+	−	−
Novus Biologicals, NLS2095	19 aa peptide from C-terminus of human HCAR1	+	+	§	§
Novus Biologicals, NBP1–51956	C-QQLARQARMKKATR (internal region)	+	+	§	§

Experiments were performed in brain slices of cortex, hippocampus, and cerebellum. +, positive signal/band; −, negative/absence of signal/band; IHC, immunohistochemistry; WB, Western blot; §, not tested. See Table 1-1, available at https://doi.org/10.1523/JNEUROSCI.2092-18.2019.t1-1, and Table 1-2, available at https://doi.org/10.1523/JNEUROSCI.2092-18.2019.t1-2.

ual neurons were simultaneously analyzed in the field of view. Intracellular calcium was measured using Fluo-8 AM (5 μM; Abcam) loaded for 15 min at 37°C, in a HEPES-buffered balanced solution containing the following (in mM): NaCl 160, KCl 5.4, HEPES 20, $CaCl_2$ 1.3, $MgSO_4$ 0.8, NaH_2PO_4 0.78, and glucose 20, pH 7.4 (adjusted with NaOH), supplemented with 0.1% Pluronic F127 (Thermo Fisher Scientific). Fluorescence was excited at 490 nm and detected at >515 nm, with an acquisition rate of 6–7 Hz. Fluorescence intensity was measured over time in regions of interest delineating neuronal soma using MetaFluor software. Calcium transients were analyzed using Mini Analysis version 6.0.3 (Synaptosoft; RRID: SCR_002184), which includes an algorithm for the detection of complex and multiple events, giving the possibility to detect overlapping or closely occurring peaks, thus allowing the analysis of the frequency of spontaneous calcium spikes under different experimental conditions.

FRET measurements of intracellular cAMP levels were measured in cells expressing Epac2-camps 48 h after transfection on an epifluorescence inverted microscope (Zeiss) equipped with an image splitter (DV2, Photometrics), using a high numerical aperture fluorescence objective (40×, 1.3 NA, oil-immersion). Fluorescence excitation wavelengths were selected via fast holographic monochromator (Polychrome II, Till Photonics) coupled to a xenon lamp, and fluorescence was detected using an EMCCD camera (LUCA-R, Andor). Digital image acquisition was performed using the MetaFluor software. One individual neuron was imaged in the selected field of view. Fluorescence was excited at 430 nm, and detected at 475 and 530 nm for cyan fluorescent protein (CFP) and yellow fluorescent protein (YFP), respectively, with an acquisition rate of 0.2 Hz. Regions of interest were selected from single cell YFP and CFP images. The FRET ratios (CFP/YFP) were computed using MetaFluor software. Decrease in FRET ratio signal reflects a decrease in the intracellular cAMP levels.

Electrophysiological recordings. Patch-clamp recordings were made using borosilicate glass pipettes (5–6 MΩ) filled with intracellular solution containing the following (in mM): K-gluconate 135, NaCl 5, Na-phosphocreatine 5, $MgCl_2$ 1, EGTA 1, HEPES 10, Mg-ATP 2, and Na_3-GTP 0.4, pH 7.2 (adjusted with KOH). Recordings were made with a MultiClamp 700B amplifier (Molecular Devices). Data were acquired with a Digidata 1440A digitizer (Molecular Devices), at 10 kHz sampling rate, controlled with pCLAMP 10 software (RRID:SCR_011323), and analyzed with Clampfit (RRID:SCR_011323) and Mini Analysis (RRID: SCR_002184). The criterion for experiment inclusion was based on the verification of stable access resistance and leak current (<200 pA at −70 mV in control solution).

mEPSCs were recorded at −70 mV in voltage clamp in gap-free mode. A stabilization period of 5 min was routinely allowed after establishment of the whole-cell configuration. Experiments were performed in presence of 1 μM tetrodotoxin (TTX) and 60 μM bicuculline. mEPSCs were recorded for 10 min in the absence and presence of HCAR1 agonist and the last 5 min were analyzed. Cells included in the analysis had a membrane potential less than or equal to −55 mV, stable access resistance, and recovery after washout.

We further assessed cell passive properties and firing frequency of WT neurons in control conditions and after HCAR1 activation. The resting membrane potential (RMP) was measured in current-clamp mode after the whole-cell configuration was established. The input resistance (R_N) was determined from the linear slope of the current–voltage relationship around the RMP, obtained by a series of 160 ms current steps (starting at −140 pA with 30 pA increments). The rheobase was determined as the minimal current amplitude able to evoke an action potential (AP) and was obtained by applying 3 s steps of positive current (starting at 0 pA, with 50 pA increments). The firing frequency was assessed as the number of AP evoked in response to 1 s current injection steps (0–450 pA, with 50 pA increments). AP frequency was measured as the number of APs in response to 150 pA current injection. The membrane time constant was estimated by fitting an exponential function to a voltage step of −5 mV.

Table 2. Summary of behavioral phenotype of WT versus HCAR1 KO

		WT	*n*	HCAR1 KO	*n*
(1)	Weight (g)	26.3 ± 0.4	12	27.4 ± 0.9 n.s.	12
	Food consumption (g)	3.5 ± 0.3	10	3.3 ± 0.2 n.s.	10
	Water consumption (ml)	3.1 ± 0.2	10	3.7 ± 0.3 n.s.	10
	Total travel distance (cm)	55,374 ± 7352	10	52,059 ± 5197 n.s.	10
	Dark phase	41,985 ± 5419		43,263 ± 4515 n.s.	
	Light phase	13,389 ± 2885		8796 ± 2224 n.s.	10
	Total time in the nest (min)	46,136 ± 3363	10	47,686 ± 3442 n.s.	10
	Dark phase	21,681 ± 1781		20,962 ± 2537 n.s.	
	Light phase	24,454 ± 1785		26,724 ± 1369 n.s.	
(2)	Rearing (number/min)	8.6 ± 0.7	12	9.8 ± 0.5 n.s.	12
	Number of grooming (number/min)	0.6 ± 0.1	12	0.6 ± 0.1 n.s.	12
	Grooming duration (s)	24 ± 5.3	12	25 ± 5.5 n.s.	12

Data are shown as the mean ± SEM. Experiments were performed on independent animals. (1), PhenoTyper cage observations; (2), free observations; n.s., not significant (Student's unpaired *t* test).

Paired pulse ratio (PPR) experiments were measured using a pipette solutions containing the following (in mM): CsF 121.6, CsCl 8.4, Na-phosphocreatine 5, EGTA 1, HEPES 10, Mg-ATP 2, Na_3-GTP 0.4, and QX-314Cl 1, pH 7.2 (adjusted with CsOH). Neurons were voltage-clamped at −70 mV in the whole-cell configuration. Stimulation was performed using a Pt-Ir concentric bipolar electrodes (tip diameter, 2–3 μm; model CEA3, MicroProbes for Life Science) placed near the recorded neuron and connected to an Iso-Flex stimulus isolator (A.M.P.I.). The minimum stimulation intensity able to trigger a single evoked EPSC was determined in the range 0.4–1 mA. Two consecutive 1 ms stimuli were applied with an interval of 50 ms.

Solutions and drugs. CO_2/bicarbonate-buffered experimental solutions contained the following (mM): NaCl 135, KCl 5.4, $NaHCO_3$ 25, $CaCl_2$ 1.3, $MgSO_4$ 0.8, NaH_2PO_4 0.78, and glucose 5, bubbled with 5% CO_2/95% air. Glucose was maintained in a nonlimiting fashion (5 mM) in all solutions. Control extracellular solutions and solutions containing tested drugs were gravity fed at 1 ml/min and at 35°C. The pH of CO_2-equilibrated solutions was 7.4 and was not altered by the added L-lactate (Bozzo et al., 2013). L-Lactate, 3,5-dihydroxybenzoic acid (3,5-DHBA), 3-chloro-5-hydroxybenzoic acid (3Cl-HBA), 9-(tetrahydro-2-furany)-9H-purin-6-amine (SQ 22536), baclofen, guanfacine, gallein, and QX-314Cl were obtained from Sigma-Aldrich. H-89 dihydrochloride (H-89), N_6-cyclopentyladenosine (CPA), (1-[6-[[(17β)-3-methoxyestra-1,3,5(10)-trien-17-yl]amino]hexyl]-1H-pyrrole-2,5-dione; U73122), and bi-

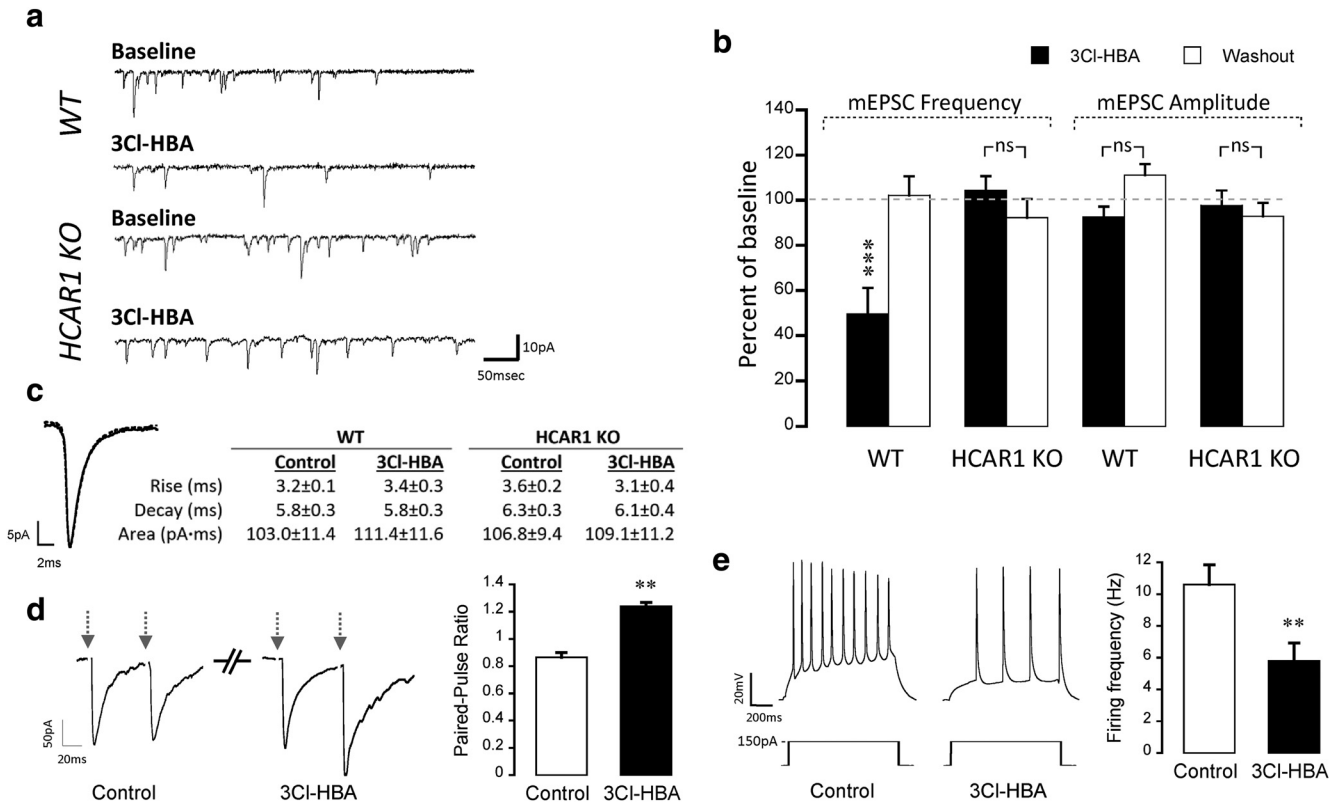

Figure 2. HCAR1 activation decreases mEPSC frequency and modulates intrinsic membrane properties of mouse cortical neurons. ***a***, Representative mEPSCs traces from a neuron recorded in the presence and in the absence of 3Cl-HBA 40 μM for WT and HCAR1 KO. Voltage-clamp recordings of mEPSCs were performed in the presence of TTX (1 μM) and bicuculline (60 μM) with neurons clamped at −70 mV. ***b***, Summary of mEPSC frequency and amplitude (percentage of baseline) in response to 3Cl-HBA application in WT ($n = 7$) and HCAR1 KO neurons ($n = 6$). A depression of mEPSC frequency, but not amplitude, was observed upon HCAR1 activation in neurons prepared from WT mice but not from HCAR1 KO mice. ***c***, Representative superimposed averaged traces of 1000 events from the same WT neuron in the absence (full line) and in the presence of 3Cl-HBA (dotted line), and a table showing corresponding average kinetic values of all events from WT and KO in the presence and in the absence of 3Cl-HBA, demonstrating similar kinetics in WT and KO neurons. Significance is shown compared with baseline and among conditions. ***d***, Left, Representative responses to paired pulse protocols using an interstimulus interval of 50 ms in WT neurons before and after HCAR1 activation (left). Arrows represent the stimulation. Right, Summary graph of PPR results ($n = 7$). Significance is shown between the control condition and after 3Cl-HBA application. ***e***, Representative traces from neurons recorded before and after HCAR1 activation (left), obtained from a series of current injections (0–450 pA, 1 s, 50 pA increments); the response to 150 pA current injection is shown. Summary graph (right) of the effect of HCAR1 activation on neuronal firing frequency following steps of current injection ($n = 5$). The firing frequency (in Hz) was calculated from the number of AP evoked by a 150 pA current injection. Significance is shown between the control and 3Cl-HBA conditions. $^{**}p < 0.01$, $^{***}p < 0.001$, ns, not significant.

Table 3. Effect of HCAR1 activation on passive properties of cortical cultured neurons

	Control	3Cl-HBA 40 μM
RMP (mV)	−59.3 ± 1.1	−62.9 ± 1.3*
R_N (MΩ)	97.3 ± 6.4	77.5 ± 6.2*
Rheobase (pA)	78.6 ± 6.8	93.6 ± 8.7*
Time constant (ms)	16.4 ± 1.1	18.8 ± 0.5*

Data are shown as the mean ± SEM. Experiments were performed in five independent WT neurons. All parameters were tested in all cells used for analysis.

*$p < 0.05$ Student's paired *t* test.

cuculline were obtained from Tocris Bioscience. Forskolin was obtained from Biomol and TTX was obtained from BioTrend. All drugs were diluted in CO_2/bicarbonate-buffered solution to their final concentration and perfused in the same conditions as the control.

Experimental design and statistical significance. Immunohistochemistry data quantification was performed using ImageJ software (RRID: SCR_003070). We first identified Hoechst-stained nuclei in the field, allowing us to assess the number of cells. We then determined cells that were NeuN-positive and/or mRFP-positive to assess the number of neurons that were expressing mRFP. For each independent experiment, three different fields of view were analyzed. The result of the quantification is shown as the percentage of Hoechst-positive cells.

To assess the HCAR1 functional role in neuronal activity, experiments were performed using a sequential application of drugs. Each individual experiment represents responses obtained by the application of the tested drugs, one following the other, on the same cells followed by washout with the control solution. Statistical analyses were performed using KaleidaGraph software (Synergy Software; RRID:SCR_014980). Data are the mean ± SEM and are represented as the percentage compared with control; *n* represents the number of independent experiments. Data normality was checked using the Shapiro–Wilk test.

When more than one condition was tested on the same experiment, comparisons were made using one-way ANOVA followed by Bonferroni correction for each experimental group to assess statistical significance against respective control, and among the tested conditions. When only one condition was tested, the paired or nonpaired *t* test was performed to assess statistical significance ($^{*}p < 0.05$, $^{**}p < 0.01$ and $^{***}p < 0.001$). Only experiments where the effect of the tested drugs could be washed out were taken into consideration for analysis.

Results

HCAR1 expression in neurons

Localization of HCAR1 protein in neurons has been reported by us and other research groups based on immunohistochemistry (Bozzo et al., 2013; Lauritzen et al., 2014). In this study, qRT-PCR was used to assess HCAR1 mRNA expression in primary neuronal cultures at DIV 14 (Fig. 1*a*) from WT mice. Figure 1*b* shows genotyping results of WT and HCAR1 KO mice. In the gene construct of HCAR1 KO mice, the coding sequence of HCAR1

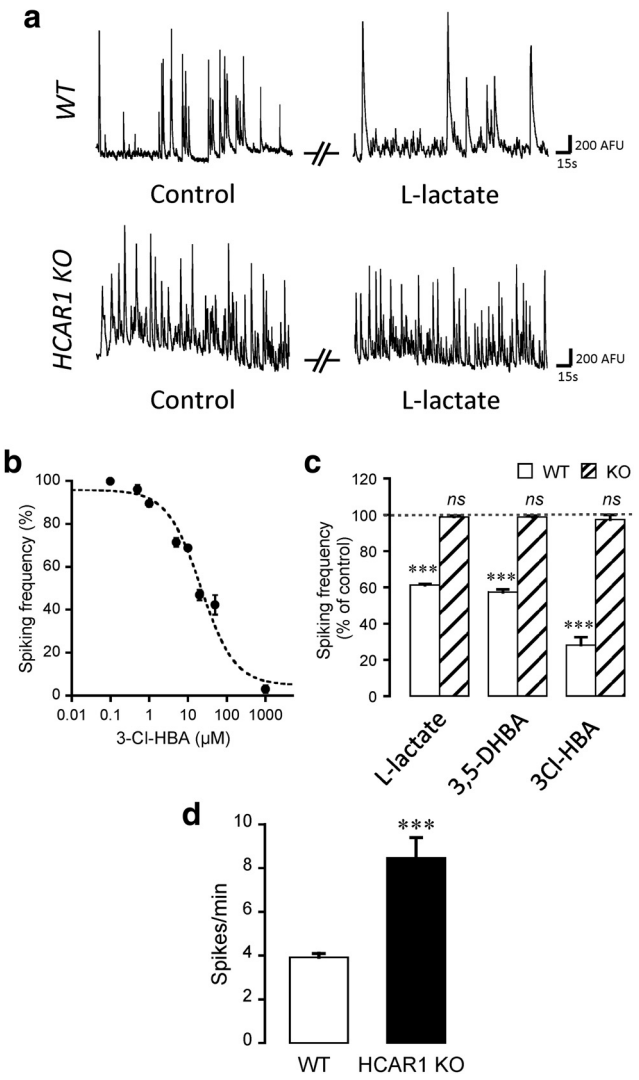

Figure 3. Effect of neuronal activation in neuronal calcium spiking activity. ***a***, Representative traces of calcium spiking in control or 5 mM l-lactate-containing solutions, for both WT and HCAR1 KO neurons. ***b***, The effect of the HCAR1 agonist 3Cl-HBA on spontaneous calcium activity of neurons was concentration dependent, with an IC_{50} value of 21.5 ± 6.1 μM ($n = 177$ neurons from 23 experiments). The IC_{50} value was obtained by nonlinear curve fitting using the Levenberg-Marquardt algorithm. ***c***, Effect of HCAR1 activation on calcium spiking frequency from WT and HCAR1 KO neurons with 5 mM L-lactate (WT: $n = 66$ cells, 16 experiments; HCAR1 KO: $n = 81$ cells, 16 experiments), 1 mM 3,5-DHBA (WT: $n = 57$, 16 experiments; HCAR1 KO: $n = 74$ cells, 12 experiments), or 40 μM 3Cl-HBA (WT: $n = 31$ cells, 3 experiments; HCAR1 KO: $n = 32$ cells, 5 experiments). Spiking frequency is shown as a percentage of activity measured in the control condition. The effect of HCAR1 activation was reversible in all experiments (data not shown). Significance is shown compared with control and among conditions. ***d***, Comparison of basal spontaneous spiking frequencies of neurons from WT ($n = 16$) and HCAR1 KO ($n = 16$) mice. ***$p < 0.001$, ns, not significant.

was replaced by a cassette containing the lacZ and the neomycin resistance genes (Ahmed et al., 2010). Samples from WT shows a PCR HCAR1 band corresponding to a 470 bp product, whereas the ones from HCAR1 KO animals have a neomycin-only, 800 bp product band. In the next phase, we wanted to investigate the HCAR1 protein expression and localization in primary cultured neurons. For this purpose, we took advantage of the HCAR1 KO mice, not available in our first studies, to assess the specificity of commercial antibodies. Table 1 shows that of nine commercial antibodies raised against different epitopes, tested by Western blot and/or immunohistochemistry, none displayed a convincing absence of signal in HCAR1 KO tissue. To circumvent this issue, we used a transgenic mouse that expresses mRFP under the HCAR1 promoter (Ahmed et al., 2010). This fluorescent reporter protein is not targeted to the plasma membrane but spreads in the cytoplasm, allowing us to identify the cells that endogenously express the HCAR1 transcripts. In primary neurons from mRFP-HCAR1 mice, all Hoechst-positive cells were also mRFP-HCAR1 positive. Among these cells, ~80% were also positive for NeuN (Fig. 1*c*,*d*). This result indicates that these cultured neurons express mRFP-HCAR1. The 20% of the cells that were mRFP-HCAR1 positive, but NeuN negative, could represent cells that are not mature neurons and that also express HCAR1.

HCAR1 KO animals show normal general behavior

According to previous studies, HCAR1 KO mice do not show obvious abnormalities when compared with WT mice, which includes no difference in body weight (Ahmed et al., 2010) or locomotion when exposed to high-intensity interval exercises (Morland et al., 2017). We extended the phenotype analysis and performed a basic behavioral neurological screening in these animals. We did not find differences in the quantitative observations obtained with the PhenoTyper cage or during the free observation (Table 2). Neither WT nor HCAR1 KO animals presented traces of compulsive licking, self-destructive biting, retropulsion, or convulsions. No differences were observed in the grip strength test ($t_{(22)} = 0.49$, $p = 0.63$, unpaired *t* test) and in the hindpaw clasping test (none of the mice failed the test; WT, $n = 12$ animals; HCAR1 KO, $n = 12$ animals).

Activation of HCAR1 decreases mEPSC frequency and excitability

In the next phase, we evaluated the effects of HCAR1 activation on basal neurotransmission using the whole-cell patch-clamp technique. Figure 2*a* shows representative electrophysiological traces of mEPSCs recorded from neurons of WT and HCAR1 KO mice. We observed a significant decrease (~50%) in mEPSC frequency in the WT group during HCAR1 activation by its agonist 3Cl-HBA (40 μM; $F_{(2,6)} = 12.92$, $p = 0.0013$, ANOVA). 3Cl-HBA application did not alter the mean amplitude ($F_{(2,6)} = 5.84$; $p = 0.562$, ANOVA) or kinetics (rise: $t_{(6)} = -1.41$, $p = 0.22$; decay: $t_{(6)} = 0.19$, $p = 0.85$; area: $t_{(6)} = -0.77$, $p = 0.48$, paired *t* test) of mEPSCs (Fig. 2*b*,*c*). Importantly, the frequency ($F_{(2,5)} = 0.09$, $p = 1$, ANOVA), amplitude ($F_{(2,5)} = 0.23$, $p = 1$, ANOVA), and kinetics (rise: $t_{(5)} = 1.39$, $p = 0.22$; decay: $t_{(5)} = 0.87$, $p = 0.42$; area: $t_{(5)} = -0.63$, $p = 0.56$, paired *t* test) of mEPSCs were not influenced by HCAR1 activation in neurons from HCAR1 KO mice (Fig. 2*c*). These results are a first indication of a presynaptic mechanism induced by HCAR1. To further test this hypothesis, we performed a PPR experiment before and after HCAR1 activation. These experiments revealed a significant increase in the PPR value ($t_{(6)} = -5.18$, $p = 0.002$, paired *t* test; Fig. 2*d*), supporting the notion that HCAR1 has a presynaptic component.

However, previous works indicated that HCAR1 activation modulates passive properties and decreases the firing frequency of rat CA1 pyramidal neurons (Herrera-López and Galván, 2018). Thus, we investigated whether HCAR1 activation could modulate intrinsic properties of mouse cortical neurons as well. We observed that the activation of HCAR1 with 3Cl-HBA (40 μM) decreased firing frequency by 45% ($t_{(4)} = 6.53$, $p = 0.003$, paired *t* test; Fig. 2*e*), as previously observed by Herrera-López and Galván (2018). Table 3 further shows that the activation of HCAR1 causes a significant decrease in R_N ($t_{(4)} = 4.35$, $p = 0.01$, paired *t* test) and membrane time constant ($t_{(4)} = -3.69$, $p = 0.02$, paired *t* test) increases the rheobase current ($t_{(4)} = -4.09$, $p = 0.01$, paired *t* test), and hyperpolarizes the RMP ($t_{(4)} = 3.41$,

$p = 0.03$, paired t test). These experiments indicate that HCAR1 activation induces changes in the intrinsic membrane properties of mouse cortical neurons, eliciting a decrease in excitability in addition to a presynaptic mechanism.

Activation of HCAR1 decreases neuronal calcium spiking frequency

The spontaneous spiking activity of primary cortical neurons was then measured by calcium imaging. As previously demonstrated (Bozzo et al., 2013), intracellular calcium transients directly correlate with action potentials in single neurons. This approach offers the advantage of recording a number of cells in parallel without altering the intracellular solute composition compared with the whole-cell patch-clamp method.

Activation of HCAR1 was tested in neurons obtained from both WT and HCAR1 KO mice. HCAR1 is endogenously activated by L-lactate in neurons with an apparent IC_{50} of 4.2 mM (Bozzo et al., 2013). For these experiments, we tested the endogenous ligand L-lactate, as well as two specific nonmetabolized agonists of HCAR1, namely, 3,5-DHBA and the newer, higher affinity agonist 3Cl-HBA. Figure 3*a* shows that application of L-lactate (5 mM) on neurons from WT mice led to a decrease in spontaneous spiking frequency by ~40%, as observed previously (Bozzo et al., 2013). We then tested the higher-affinity agonist 3Cl-HBA and performed a log-dose analysis of its effect on neuronal activity (Fig. 3*b*). 3Cl-HBA caused a decrease in spiking frequency with an IC_{50} of 21.6 ± 6.1 μM ($n = 23$ experiments), virtually identical to the 22 μM potency originally found with the mouse HCAR1 isoform (Dvorak et al., 2012). Figure 3*c* summarizes this series of experiments and shows that L-lactate ($F_{(2,15)} = 555.95$, $p < 0.0001$, ANOVA), 3,5-DHBA ($F_{(2,15)} = 429.20$, $p < 0.0001$, ANOVA), and 3Cl-HBA ($F_{(2,2)} = 224.57$, $p < 0.0001$, ANOVA) strongly decreased spiking frequency. In sharp contrast, L-lactate ($F_{(2,15)} = 45.71$, $p = 0.26$, ANOVA), 3,5-DHBA ($F_{(2,11)} = 47.59$, $p = 0.22$, ANOVA), or 3Cl-HBA ($F_{(2,4)} = 3.93$, $p = 1$, ANOVA) did not alter the spontaneous spiking frequency in neurons prepared from HCAR1 KO mice. This result is a strong indication that HCAR1 activation is responsible and required for the modulatory effects of L-lactate on neuronal network spontaneous activity. It should be added that in control conditions, neurons obtained from HCAR1 KO displayed an approximately twofold higher basal activity compared with WT neurons ($t_{(30)} = -4.83$, $p < 0.0001$, unpaired t test; Fig. 3*d*), suggesting that HCAR1 might have a role in the tonic inhibition of neuronal activity.

Intracellular HCAR1 signaling pathways in neurons

HCA receptors have been reported to be coupled to G_i proteins in the adipose tissue (Liu et al., 2009). Our group previously demonstrated that the lactate effect on cortical neurons is sensitive to pertussis toxin, which supports the notion that HCAR1 in neurons decreases neuronal activity through the G_i-protein pathway (Bozzo et al., 2013). Therefore, we investigated whether the downstream effectors of G_i-protein were involved in the decrease of neuronal activity induced by HCAR1 activation.

Using calcium imaging, we analyzed the effect of HCAR1 activation on neuronal spiking frequency upon pharmacological manipulation of the intracellular pathways known to follow the activation of G_i-proteins. Activation of AC by forskolin (10 μM) caused an ~30% increase in spiking activity in WT neurons, which was reversed by concomitant activation of HCAR1 ($F_{(3,4)} = 23.16$, $p < 0.0001$, ANOVA; Fig. 4*a*). In comparison, forskolin was found to have a stronger stimulatory effect on neurons from

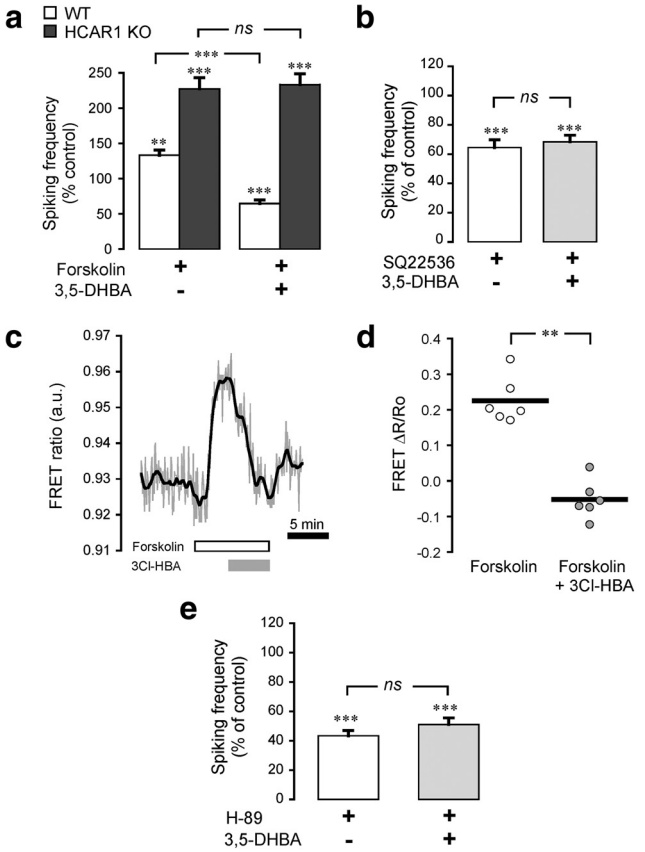

Figure 4. Adenylyl cyclase, cAMP, and PKA involvement in neuronal HCAR1 signaling. ***a***, Activation of AC with forskolin (10 μM) increased spiking activity in both WT ($n = 44$ cells, 5 experiments) and HCAR1 KO ($n = 29$ cells, 3 experiments) neurons compared with their respective baseline activity. ***b***, Application of 3,5-DHBA (1 mM), in sequence with forskolin, decreased spiking activity in WT, but not in HCAR1 KO neurons. Inhibition of AC with SQ22536 (10 μM) decreased spiking activity in WT neurons ($n = 46$ cells, 6 experiments). Application of 3,5-DHBA, in sequence with SQ22536, caused no further decrease in neuronal activity. ***c***, Representative trace of the effects of HCAR1 activation on cAMP levels measured using the Epac2-camps FRET sensor. The FRET (CFP/YFP) ratio, proportional to the cAMP levels, is shown for a single neuron along the timeline. Application of the AC activator forskolin (10 μM) caused a rapid signal rise, and the subsequent HCAR1 activation using 3Cl-HBA (40 μM) reversed this increase. ***d***, Summary of absolute FRET ratio values in the presence of forskolin before and after stimulation of HCAR1 using 3Cl-HBA. The graph shows individual values plotted along with the mean value of all experiments ($n = 6$ cells, 6 experiments). ***e***, Inhibition of PKA with H-89 (1 μM) decreased spiking activity in WT neurons ($n = 64$ cells, 6 experiments). Application of 3,5-DHBA, in sequence with H-89, did not further decrease neuronal activity. Significance is shown compared with control and among conditions in ***a***, ***b***, and ***e***. $^{**}p < 0.01$, $^{***}p < 0.001$, ns, not significant.

HCAR1 KO animals, suggesting a tonic inhibitory effect operated by HCAR1 on AC. Moreover, the HCAR1 agonist 3,5-DHBA had no effect on the forskolin-induced activity of these neurons ($F_{(3,2)} = 24.89$, $p = 1$, ANOVA; Fig. 4*a*). Conversely, the inhibition of AC with SQ22536 (10 μM) decreased neuronal spiking activity by ~40%. In this situation, under AC inhibition, HCAR1 activation did not cause further spiking activity decrease ($F_{(3,6)} = 15.39$, $p = 1$, ANOVA; Fig. 4*b*). These results indicate that HCAR1 activation impacts AC in neurons. Live-cell imaging of cAMP levels in neurons was then performed using the FRET sensor Epac2-camps. Figure 4*c* shows that forskolin application caused a rapid increase in FRET response, corresponding to cAMP level rise. This cAMP level increase was efficiently reversed by the application of the HCAR1 agonist 3Cl-HBA ($t_{(5)} = 6.62$, $p = 0.001$, paired t test; Fig. 4*c*,*d*). We then tested PKA as one of the main

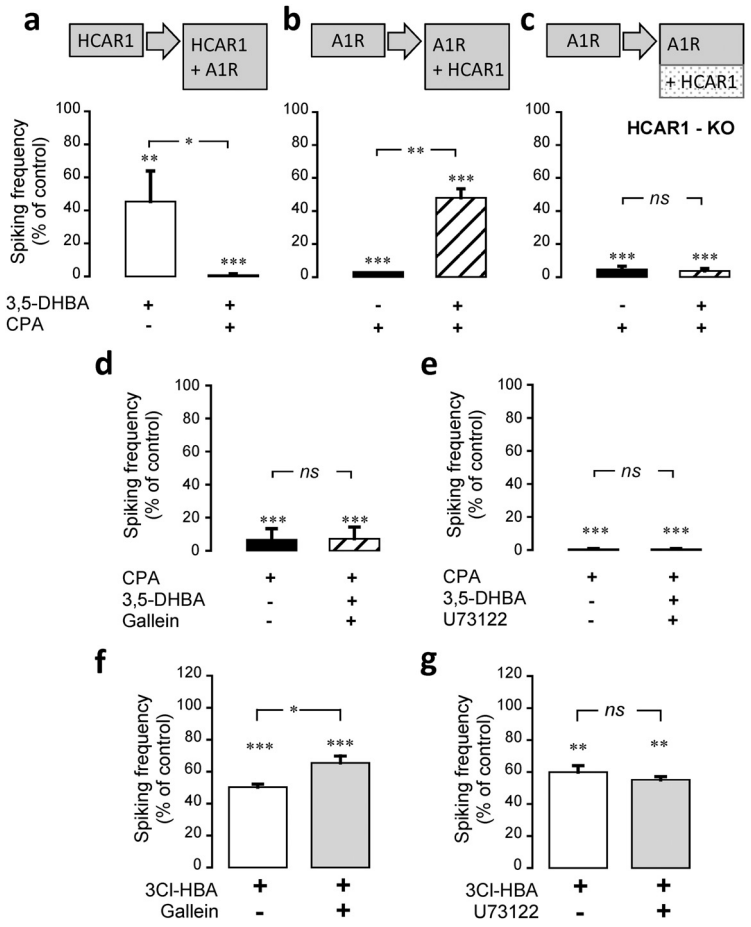

Figure 5. HCAR1 interaction with other G_i-coupled receptors for the modulation of neuronal activity. ***a***, HCAR1 was first activated using 3,5-DHBA (1 mM) and in a second phase, the agonist of A1R, CPA (30 nM), was coapplied, which caused a stronger decrease in spiking activity compared with HCAR1 activation alone. The same protocol was performed with a reverse order of receptor activation (i.e., first CPA and then 3,5-DHBA application). ***b***, ***c***, Although the secondary 3,5-DHBA application caused a partial reversal of inhibition in neurons from WT animals (***b***), it had no effect on neurons from HCAR1 KO animals (***c***). ***d***, ***e***, The effect of the coactivation of A1R with HCAR1 in the presence of gallein (10 μM), a $\beta\gamma$ subunit signaling inhibitor (***d***), or U73122 (10 μM), a PLC blocker (***e***), is shown. Both treatments prevented the partial reversal of inhibition observed in ***b***. ***f***, ***g***, Effect of $\beta\gamma$ subunit inhibition using gallein (10 μM; ***f***) and of PLC blockade with U73122 (10 μM; ***g***) on HCAR1 activation alone using 3Cl-HBA-HBA (40 μM). Inhibition of $\beta\gamma$ subunit partially reverted HCAR1 effect on neural activity; however, PLC blockade did not influence the HCAR1 effect. Data are the mean ± SEM from 21 cells, 4 experiments (***a***); 20 cells, 4 experiments (***b***); 27 cells, 4 experiments (***c***); 26 cells, 4 experiments (***d***); 14 cells, 3 experiments (***e***); 33 cells, 4 experiments (***f***); and 22 cells, 3 experiments (***g***). Significance is shown compared with control and among conditions. *$p < 0.05$, **$p < 0.01$, ***$p < 0.001$, ns, not significant.

downstream targets of AC-cAMP. To this aim, we used H-89 (1 μM) to inhibit PKA, which led to a decrease in neuronal network activity. Under PKA blockade, the activation of HCAR1 using 3,5-DHBA did not cause a further decrease in spiking activity ($F_{(3,6)} = 80.75$, $p = 0.61$, ANOVA; Fig. 4*e*). Together, these experiments demonstrate that HCAR1 action on neuronal spiking activity involves the inhibition of AC, causing a decrease in cAMP levels and in turn of PKA activity.

HCAR1 interacts with G_i-coupled receptors to modulate neuronal activity

A characteristic feature of GPCRs is their ability to cross talk with other GPCRs at the level of their intracellular pathways (Werry et al., 2003). These interactions significantly complexify their effects on cellular or network targets. We therefore asked whether HCAR1 is capable of functionally interacting with other G_i-coupled receptors, such as the adenosine A1 receptor (A1R), the $GABA_B$ receptor ($GABA_BR$), and the α_{2A}-adrenoreceptor ($\alpha_{2A}R$). To address this question, we used calcium imaging to monitor neuronal activity upon the sequential activation of HCAR1 and one of the G_i-coupled receptors. We found that the activation of HCAR1 with 3,5-DHBA decreased neuronal spiking frequency, as shown above, and the subsequent coactivation of HCAR1 and A1R using CPA induced a further decrease in neuronal spiking frequency ($F_{(3,3)} = 20.57$, $p = 0.046$, ANOVA; Fig. 5*a*). After washout of the drugs, spiking activity returned to its original frequency (data not shown). The same apparent additive inhibition of spiking was observed when investigating the cooperation of HCAR1 with $GABA_BR$ or with $\alpha_{2A}R$, which were activated using baclofen and guanfacine, respectively (Table 4). It is expected that if the activation of HCAR1 and the other G_i-coupled receptors are independent, reversing the order of agonist application should result in the same combined inhibition of neuronal spiking. We tested this hypothesis by first stimulating A1R and immediately after coactivating HCAR1. Unexpectedly, when A1R was first activated, the subsequent coactivation of HCAR1 partially reversed the inhibition induced by A1R alone ($F_{(3,3)} = 32.09$, $p = 0.007$, ANOVA; Fig. 5*b*). We repeated the same protocol with $GABA_BR$ or $\alpha_{2A}R$, and the same pattern was observed (Table 4). To ascertain that this effect was specifically brought about by HCAR1, we repeated these experiments with neurons prepared from HCAR1-KO animals. Figure 5*c* ($F_{(3,3)} = 193.06$, $p = 1$, ANOVA) and Table 4 show that in neurons lacking HCAR1, no such interaction was observed, indicating that the observed effects were indeed mediated by the HCAR1. We then asked whether this reversal effect caused by HCAR1 activation was generic to all G_i-coupled receptors. We repeated the experiments depicted above for A1R/$GABA_BR$, A1R/$\alpha_{2A}R$, and $\alpha_{2A}R$/$GABA_BR$ pairs. The results listed in Table 5 indicate that this reversal of inhibition was not observed among these receptor pairs, which did not recapitulate the observations made with HCAR1. This indicates that this reversal of frequency decrease is a distinct property of HCAR1 activation.

Overall, these experiments revealed that, depending on which receptor is activated first in sequence, different levels of inhibition of spiking frequency are obtained upon HCAR1 coactivation with other G_i-coupled receptors, highlighting the complexity of the modulation of neuronal activity operated by HCAR1.

The $G_{i\beta\gamma}$–PLC pathway is involved in the interaction of HCAR1 with G_i-coupled receptors

Although the G_i pathway is classically known for its ability to inhibit AC, both $G_{i\alpha}$ and $G_{i\beta\gamma}$ subunits can transduce signals. One of the key effectors directly regulated by $G_{\beta\gamma}$ subunits is PLC. PLC catalyzes the hydrolysis of phosphatidylinositol 4,5-

Table 4. HCAR1 interactions with $GABA_B$ and α_{2A} receptors and neuronal activity

	WT		HCAR1 KO	
	Frequency (%)	n_{cells}, n_{exp}	Frequency (%)	n_{cells}, n_{exp}
$GABA_BR$/HCAR1				
3,5-DHBA[a]	32.3 ± 6.9	37, 4		
→ + baclofen	2.6 ± 3.3*			
Baclofen	13.9 ± 0.8	12, 3	53.2 ± 3.4	35, 4
→ + 3,5-DHBA	43.6 ± 5.5*		51.7 ± 4.5 n.s.	
α_{2A}R/HCAR1				
3,5-DHBA	48.4 ± 8.9	44, 4		
→ + Guanfacine	8.4 ± 3.3*			
Guanfacine	24.2 ± 2.8	36, 4	26.8 ± 8.4	29, 4
→ + 3,5-DHBA	54.2 ± 4.1*		27.2 ± 8.2 n.s.	

Data are expressed as the percentage of the frequency observed in baseline conditions and as the mean ± SEM. n.s., not significant ANOVA, Bonferroni correction, for *n* cells from *n* experiments. Statistical significance is indicated for comparisons between the two displayed conditions.

[a]Concentrations used: 1 mm 3,5-DHBA, 0.5 μM baclofen, and 10 μM guanfacine.

*$p < 0.05$.

Table 5. Lack of functional interactions among A1, $GABA_B$, and α_{2A} receptors

	Frequency (%)	n_{cells}, n_{exp}
A1R/$GABA_BR$		
CPA[a]	2.4 ± 2.1	20, 3
→ + baclofen	1.8 ± 1.6 n.s.	
Baclofen	41.5 ± 7.6	18, 3
→ + CPA	2.7 ± 0.2*	
A1R/α_{2A}R		
CPA	8.9 ± 8.8	19, 3
→ + Guanfacine	8.4 ± 3.3 n.s.	
Guanfacine	39.2 ± 8.3	17, 3
→ + CPA	3.8 ± 1.9*	
α_{2A}R/$GABA_BR$		
Guanfacine	51.2 ± 11.6	16, 3
→ + Baclofen	42.4 ± 9.8 n.s.	
Baclofen	60.1 ± 5.4	18, 3
→ + Guanfacine	41.6 ± 7.5 n.s.	

Data are expressed as a percentage of the frequency observed in baseline conditions or as the mean ± SEM. n.s., not significant. ANOVA, Bonferroni correction, for *n* cells from *n* experiments. Statistical significance indicated for comparisons between the two displayed conditions.

[a]Concentrations used: 30 nm CPA, 0.5 μM baclofen, and 10 μM guanfacine.

*$p < 0.05$.

Table 6. Mechanism of HCAR1 interaction with $GABA_B$ and α_{2A} receptors

	Frequency (%)	n_{cells}, n_{exp}
$GABA_BR$/HCAR1		
Baclofen[a]	41.5 ± 7.6	13, 3
→ + 3,5-DHBA + gallein	41.3 ± 6.96 n.s.	
Baclofen	36.6 ± 16.2	19, 3
→ + 3,5-DHBA + U73122	12.5 ± 2.4 n.s.	
α_{2A}R/HCAR1		
Guanfacine	40.5 ± 6.0	22, 4
→ + 3,5-DHBA + gallein	46.0 ± 6.3 n.s.	
Guanfacine	51.2 ± 11.7	17, 3
→ + 3,5-DHBA + U73122	47.5 ± 9.5 n.s.	

Data are expressed as a percentage of the frequency observed in baseline conditions or as the mean ± SEM. n.s., not significant. ANOVA, Bonferroni correction, for *n* cells from *n* experiments. Statistical significance indicated for comparisons between the two displayed conditions.

[a]Concentrations used: 1 mm 3,5-DHBA, 0.5 μM baclofen, 10 μM guanfacine, 10 μM gallein, and 10 μM U73122.

biphosphate to generate 1,2-diacylglycerol and inositol 1,4,5-trisphosphate, which binds to its receptor on the endoplasmic reticulum (Rhee, 2001). Thus, we investigated whether PLC activation induced by the $G_{i\beta\gamma}$ subunit was involved in the observed effect on the functional interaction between HCAR1 and G_i-coupled receptors. In experiments repeating the sequence of agonist application presented in Figure 5*b*, the inhibition of the $G_{i\beta\gamma}$ subunit using gallein suppressed the partial reversal of inhibition induced by the coactivation of A1R and HCAR1 ($F_{(3,3)} = 84.71$, $p = 1$, ANOVA; Fig. 5*d*). The same approach was applied to test the involvement of the $G_{i\beta\gamma}$ subunit on the cooperation observed between $GABA_BR$ or $\alpha_{2A}R$ and HCAR1. As indicated in Table 6, in both cases, gallein prevented the HCAR1 agonist from reversing the inhibition induced by $GABA_BR$ or $\alpha_{2A}R$ stimulation. In all experiments, after washout of gallein and agonists, the spiking frequency returned to its control value (data not shown). These results support the involvement of the $G_{\beta\gamma}$ subunit in the observed effects.

PLC is classically activated by the $G_{q\alpha}$- and $G_{q\beta\gamma}$-proteins dissociated from G_q-coupled receptors. However, PLC was also shown to be activated by $G_{i\beta\gamma}$-proteins released from G_i-proteins (Tomura et al., 1997; Mizuta et al., 2011). Thus, we investigated whether PLC was the downstream mechanism activated by the $G_{i\beta\gamma}$ subunit and involved in the interplay between HCAR1 and other G_i-coupled receptors. The application of U73122, the inhibitor of PLC, prevented HCAR1 agonist from reversing the spiking frequency decrease caused by A1R ($F_{(3,3)} = 1621.87$, $p = 1$, ANOVA; Fig. 5*e*), $GABA_BR$, or $\alpha_{2A}R$ (Table 6). After washout of U73122 and agonists, the spiking frequency returned to its control value (data not shown). These results indicate that the partial reversal of inhibition caused by HCAR1 activation under these conditions involves $G_{i\beta\gamma}$ and PLC. As a control, we assessed the effect of $G_{i\beta\gamma}$ and PLC blockade on the HCAR1 signaling itself. Blockade of $G_{i\beta\gamma}$ was sufficient to decrease the inhibitory action of HCAR1 ($F_{(3,3)} = 84.10$, $p = 0.008$, ANOVA; Fig. 5*f*). In contrast, the inhibition of PLC did not influence the effect of HCAR1 activation alone ($F_{(3,3)} = 59.38$, $p = 1$, ANOVA; Fig. 5*g*). Thus, it appears that the $G_{i\beta\gamma}$ subunit is necessary for the modulatory effects of HCAR1, but that PLC is only required upon activation of an additional G_i-coupled receptor. Together, these results indicate that HCAR1 interacts with G_i-coupled receptors in a complex but specific manner, through both its $G_{i\alpha}$ and $G_{i\beta\gamma}$ subunits.

Discussion

In this study, we demonstrate that HCAR1 in neurons is necessary for the modulation of spontaneous neuronal activity induced by L-lactate. We observed that HCAR1 activation with L-lactate induced a reversible decrease in the neuronal calcium spiking activity by ~40%, in line with first indications reported by our group (Bozzo et al., 2013). Activation of HCAR1 with nonmetabolized agonists 3,5-DHBA and 3Cl-HBA also decreased neuronal calcium spiking, as well as the mEPSCs frequency and AP firing frequency by similar amounts. We observed that HCAR1 activation induced changes in PPR and modulated neuronal intrinsic properties. As decisive arguments for the critical role of HCAR1, the activity of HCAR1 KO neurons was totally insensitive to HCAR1 agonists and the basal activity of these neurons was higher than that of neurons from WT mice. HCAR1 is therefore required for the nonmetabolic effects of L-lactate on spontaneous and tonic neuronal activity.

The HCAR1 pattern of expression in the CNS was first described to localize at the membrane of excitatory synapses of the hippocampus and cerebellar cortex (Lauritzen et al., 2014). However, because of the questionable specificity of HCAR1 antibodies currently available (Table 1; Michel et al., 2009; Wallenius et al., 2017), the precise HCAR1 cellular and regional localization in the brain remains uncertain. At this stage, one can find evidence for HCAR1 brain expression from *in situ* hybridization (the Allen

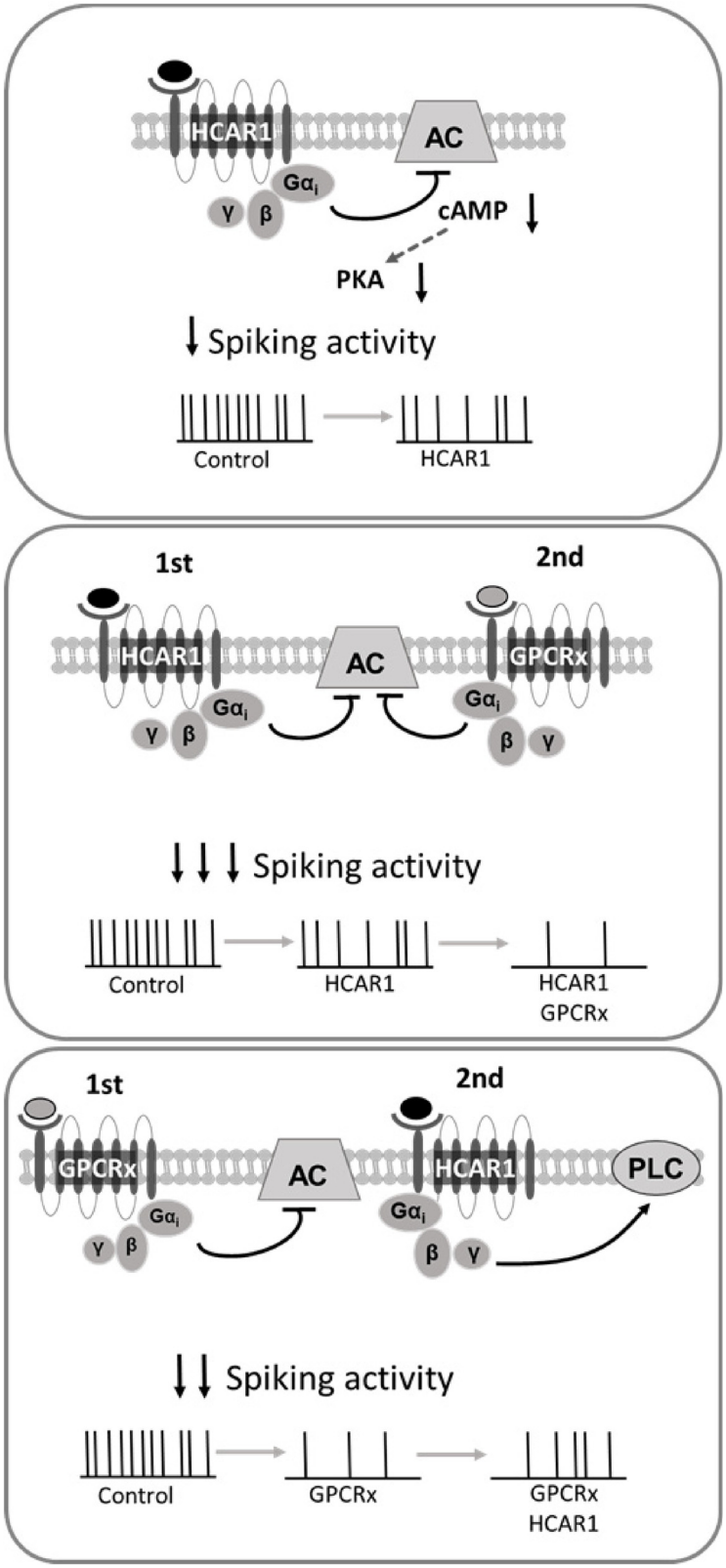

Figure 6. HCAR1 modulation of neuronal activity. Scheme depicting the modulatory effect brought about by HCAR1, when activated in isolation (Top) or with concurrent activation of other G_i-coupled GPCRs (Middle, Bottom).

Brain Atlas, http://www.brain-map.org), proteomics (UniProt database, https://www.uniprot.org), and transcriptomics (Zhang et al., 2014). HCAR1 expression in the brain was estimated to be one order of magnitude lower than in adipose tissue, where it was initially identified (Lauritzen et al., 2014).

In the CNS, several studies provided evidence for a signaling role of L-lactate. Suzuki et al. (2011) reported that long-term memory formation and maintenance are mechanisms for which L-lactate plays an essential role. Yang et al. (2014) showed that L-lactate stimulates the expression of synaptic plasticity-related genes. *In vivo* administration of L-lactate inhibited firing in the hippocampus (Gilbert et al., 2006), and in the subfornical organ 5 mM L-lactate decreased spiking activity of GABAergic neurons (Shimizu et al., 2007). A recent study showed that 5 mM L-lactate and the HCAR1 agonist 3,5-DHBA, decreased neuronal activity in a nonmetabolic way by modulating neuronal intrinsic excitability, significantly blocking fast-inactivating sodium current and increasing the delay from inactivation to a conducting state of the sodium channel in rat CA1 pyramidal neurons (Herrera-López and Galván, 2018). L-lactate also plays an important protective role in cerebral ischemia. It was observed that intracerebral L-lactate administration, decreases the lesion size and improves the neurological outcome (Berthet et al., 2009). A follow-up study showed that both L-lactate and D-lactate, which is poorly metabolized but also activates HCAR1, equally provides neuroprotection in ischemic conditions, and that 3,5-DHBA reduces cell death, suggesting that L-lactate protective functions involve HCAR1 activation (Castillo et al., 2015). HCAR1 was also shown to be involved in enhanced brain angiogenesis linked with physical activity (Morland et al., 2017).

By using electrophysiological recordings, we observed that HCAR1 activation decreased the frequency of mEPSCs, providing an indication for a presynaptic action of this receptor. This conclusion was supported by PPR experiments. To our knowledge, it is the first evidence of a presynaptic effect of HCAR1. A change in excitability has also been observed by others in rat hippocampal neurons (Herrera-López and Galván, 2018). We investigated whether this was the case in mouse cortical neurons. Activation of HCAR1 reduced R_N and firing frequency, increased the rheobase current, and caused RMP hyperpolarization. These changes in excitability possibly involve the modulation of potassium conductances and of fast inactivating sodium currents reported by Herrera-López and Galván (2018). These experiments provided evidence supporting a presynaptic as well as a postsynaptic effect of HCAR1.

In adipocytes, HCAR1 signals through a $G_{i\alpha}$-protein pathway (Ge et al., 2008) and L-lactate mediates its antilipolytic effect with

an IC_{50} value of ~5 mM (Cai et al., 2008; Liu et al., 2009). In the present study, we investigated whether in cortical neurons the $G_{i\alpha}$-protein pathway and its canonical downstream effectors were engaged for the observed inhibition of neuronal activity. Our group was able to reverse the inhibitory effect of L-lactate on neuronal activity by applying pertussis toxin, an inhibitor of $G_{i\alpha}$-proteins, which provided a first indication for the involvement of G_i-coupled receptor-mediated action of lactate in cortical neurons (Bozzo et al., 2013). Here, we found evidence for the involvement of AC, as the enhancement of spiking activity by the AC activator forskolin could be reversed by HCAR1 activation. Importantly, this did not happen in neurons from HCAR1 KO mice. Conversely, inhibiting AC using SQ22536 decreased spontaneous spiking; however, HCAR1 activation had no further effect. By directly measuring cAMP in single living neurons using a cAMP FRET biosensor, we found that the increase of cAMP level induced by AC activation was reversed by the HCAR1 agonist. This result is in agreement with the report made in rat hippocampal slices (Lauritzen et al., 2014). One important downstream target of cAMP is PKA. We found that under PKA inhibition, HCAR1 activation did no longer decrease neuronal spiking activity. Overall, these experiments indicate that the downmodulation of spontaneous neuronal activity by HCAR1 activation requires a functional intracellular AC–cAMP–PKA signaling pathway. Along these lines, cAMP is known to serve as a signal that modulates neuronal vesicular release through PKA-dependent and PKA-independent mechanisms (Seino and Shibasaki, 2005). Moreover, it is known that G_i-coupled receptors (e.g., A1R, $GABA_BR$, $\alpha_{2A}R$) regulate neuronal excitability by inducing or modulating ion currents such as various K^+ conductances, including HCN (Wang et al., 2007), two-pore domain K^+ channels (Deng et al., 2009), or GIRK channels (Breton and Stuart, 2017).

In several systems, GPCRs have the properties to interact with each other, enabling them to operate a much more complex modulation than individual transduction pathways acting independently (Werry et al., 2003). It was shown that coactivation of two $G_{i/o}$-coupled receptors (e.g., A1 adenosine and cannabinoid CB1 receptors) reduces cAMP formation in rat hippocampus, which causes additive inhibitory effects on neuronal activity (Serpa et al., 2009). Another example of intracellular interaction of combined G_i-coupled receptor activation was found between adenosine A1 and group II metabotropic glutamate receptors: their sequential activation did not lead to additive presynaptic inhibition, but to a mutual occlusion of effects on retinotectal synapses (Zhang and Schmidt, 1999).

We therefore questioned whether HCAR1 follows such interaction patterns with other classical G_i-coupled receptors. We selected the adenosine A1, $GABA_B$, and α_{2A}-adrenergic receptors, which are all G_i-coupled receptors known to be expressed in cortical neurons and to signal through the decrease of AC activity, cAMP levels, and PKA activity. When HCAR1 was stimulated first in sequence followed by the stimulation of the other GPCR, an apparent additive decrease in spiking frequency was observed. However, when the order of receptor activation was permutated, HCAR1 activation rather partly reversed the inhibitory effect of the first receptor. The observation was made with all three receptors (adenosine A1, $GABA_B$, and α_{2A}-adrenergic receptors) and was absent in HCAR1 KO neurons. This type of cooperation was not reproduced when selecting pairs among these three GPCRs. Thus, HCAR1 appears to have distinctive actions on neuronal activity when activated in combination with other receptors sharing similar transduction mechanisms.

The way HCAR1 is interacting with other GPCRs likely involves additional mechanisms than the canonical AC–cAMP–PKA pathway. It was demonstrated that recombinant HCAR1 activation induces ERK1/2 phosphorylation through the activation of its $G_{\beta\gamma}$-subunit (Li et al., 2014). HCAR1 may therefore have the ability to signal through both its $G_{i\alpha}$ and $G_{i\beta\gamma}$ subunits. We postulated that the partial reversal of inhibition of G_i-coupled receptors brought about by HCAR1 is mediated by $G_{i\beta\gamma}$ subunits released from the G_i complex after receptor stimulation. We found that blocking $G_{i\beta\gamma}$ subunit not only reduced the inhibitory effect of HCAR1 alone, but also prevented the reversal of spiking inhibition observed when HCAR1 was activated in sequence with another G_i-coupled receptor. In further support of this hypothesis, the blockade of PLC, a downstream target of $G_{\beta\gamma}$ (Katz et al., 1992), also prevented the observed partial reversal of inhibition. However, PLC seems to be engaged only when HCAR1 is activated in sequence with another receptor, since PLC blockade did not alter the effect of HCAR1 activation alone.

In this study, we demonstrate that lactate has the ability to modulate neuronal activity through HCAR1, providing further support for the hypothesis that lactate, in addition to being an energy substrate for neurons, can function as a gliotransmitter. HCAR1 mediates its effect through its $G_{i\alpha}$ subunit and its downstream effectors, resulting in a decrease of neuronal excitability and consequent firing frequency (Fig. 6). The ability of HCAR1 to functionally interact with other GPCRs through both $G_{i\alpha}$ and $G_{i\beta\gamma}$ subunits adds a level of complexity to its mechanism of action on neuronal activity and implies that the outcome of its activation *in vivo* will depend on whether other receptors of this class are active at any given time.

References

Abi-Saab WM, Maggs DG, Jones T, Jacob R, Srihari V, Thompson J, Kerr D, Leone P, Krystal JH, Spencer DD, During MJ, Sherwin RS (2002) Striking differences in glucose and lactate levels between brain extracellular fluid and plasma in conscious human subjects: effects of hyperglycemia and hypoglycemia. J Cereb Blood Flow Metab 22:271–279.

Ahmed K, Tunaru S, Tang C, Müller M, Gille A, Sassmann A, Hanson J, Offermanns S (2010) An autocrine lactate loop mediates insulin-dependent inhibition of lipolysis through GPR81. Cell Metab 11:311–319.

Barros LF (2013) Metabolic signaling by lactate in the brain. Trends Neurosci 36:396–404.

Berthet C, Lei H, Thevenet J, Gruetter R, Magistretti PJ, Hirt L (2009) Neuroprotective role of lactate after cerebral ischemia. J Cereb Blood Flow Metab 29:1780–1789.

Blad CC, Tang C, Offermanns S (2012) G protein-coupled receptors for energy metabolites as new therapeutic targets. Nat Rev Drug Discov 11:603–619.

Bozzo L, Puyal J, Chatton JY (2013) Lactate modulates the activity of primary cortical neurons through a receptor-mediated pathway. PLoS One 8:e71721.

Breton JD, Stuart GJ (2017) GABAB receptors in neocortical and hippocampal pyramidal neurons are coupled to different potassium channels. Eur J Neurosci 46:2859–2866.

Cai TQ, Ren N, Jin L, Cheng K, Kash S, Chen R, Wright SD, Taggart AK, Waters MG (2008) Role of GPR81 in lactate-mediated reduction of adipose lipolysis. Biochem Biophys Res Commun 377:987–991.

Castillo X, Rosafio K, Wyss MT, Drandarov K, Buck A, Pellerin L, Weber B, Hirt L (2015) A probable dual mode of action for both L- and D-lactate neuroprotection in cerebral ischemia. J Cereb Blood Flow Metab 35:1561–1569.

Dalsgaard MK, Quistorff B, Danielsen ER, Selmer C, Vogelsang T, Secher NH (2004) A reduced cerebral metabolic ratio in exercise reflects metabolism and not accumulation of lactate within the human brain. J Physiol 554:571–578.

Deng PY, Xiao Z, Yang C, Rojanathammanee L, Grisanti L, Watt J, Geiger JD, Liu R, Porter JE, Lei S (2009) GABA(B) receptor activation inhibits neu-

ronal excitability and spatial learning in the entorhinal cortex by activating TREK-2 K+ channels. Neuron 63:230–243.

Díaz-García CM, Mongeon R, Lahmann C, Koveal D, Zucker H, Yellen G (2017) Neuronal stimulation triggers neuronal glycolysis and not lactate uptake. Cell Metab 26:361–374.e4.

Dienel GA, Ball KK, Cruz NF (2007) A glycogen phosphorylase inhibitor selectively enhances local rates of glucose utilization in brain during sensory stimulation of conscious rats: implications for glycogen turnover. J Neurochem 102:466–478.

Dvorak CA, Liu C, Shelton J, Kuei C, Sutton SW, Lovenberg TW, Carruthers NI (2012) Identification of hydroxybenzoic acids as selective lactate receptor (GPR81) agonists with antilipolytic effects. ACS Med Chem Lett 3:637–639.

Ge H, Weiszmann J, Reagan JD, Gupte J, Baribault H, Gyuris T, Chen JL, Tian H, Li Y (2008) Elucidation of signaling and functional activities of an orphan GPCR, GPR81. J Lipid Res 49:797–803.

Gilbert E, Tang JM, Ludvig N, Bergold PJ (2006) Elevated lactate suppresses neuronal firing in vivo and inhibits glucose metabolism in hippocampal slice cultures. Brain Res 1117:213–223.

Gladden LB (2004) Lactate metabolism: a new paradigm for the third millennium. J Physiol 558:5–30.

Grishchuk Y, Ginet V, Truttmann AC, Clarke PG, Puyal J (2011) Beclin 1-independent autophagy contributes to apoptosis in cortical neurons. Autophagy 7:1115–1131.

Herrera-López G, Galván EJ (2018) Modulation of hippocampal excitability via the hydroxycarboxylic acid receptor 1. Hippocampus 28:557–567.

Husted AS, Trauelsen M, Rudenko O, Hjorth SA, Schwartz TW (2017) GPCR-mediated signaling of metabolites. Cell Metab 25:777–796.

Katz A, Wu D, Simon MI (1992) Subunits beta gamma of heterotrimeric G protein activate beta 2 isoform of phospholipase C. Nature 360:686–689.

Lauritzen KH, Morland C, Puchades M, Holm-Hansen S, Hagelin EM, Lauritzen F, Attramadal H, Storm-Mathisen J, Gjedde A, Bergersen LH (2014) Lactate receptor sites link neurotransmission, neurovascular coupling, and brain energy metabolism. Cereb Cortex 24:2784–2795.

Li G, Wang HQ, Wang LH, Chen RP, Liu JP (2014) Distinct pathways of ERK1/2 activation by hydroxy-carboxylic acid receptor-1. PLoS One 9:e93041.

Liu C, Wu J, Zhu J, Kuei C, Yu J, Shelton J, Sutton SW, Li X, Yun SJ, Mirzadegan T, Mazur C, Kamme F, Lovenberg TW (2009) Lactate inhibits lipolysis in fat cells through activation of an orphan G-protein-coupled receptor, GPR81. J Biol Chem 284:2811–2822.

Livak KJ, Schmittgen TD (2001) Analysis of relative gene expression data using real-time quantitative PCR and the 2(-δ δ C(T)) method. Methods 25:402–408.

Mächler P, Wyss MT, Elsayed M, Stobart J, Gutierrez R, von Faber-Castell A, Kaelin V, Zuend M, San Martin A, Romero-Gómez I, Baeza-Lehnert F, Lengacher S, Schneider BL, Aebischer P, Magistretti PJ, Barros LF, Weber B (2016) In vivo evidence for a lactate gradient from astrocytes to neurons. Cell Metab 23:94–102.

Michel MC, Wieland T, Tsujimoto G (2009) How reliable are G-protein-coupled receptor antibodies? Naunyn Schmiedebergs Arch Pharmacol 379:385–388.

Mizuta K, Mizuta F, Xu D, Masaki E, Panettieri RA Jr, Emala CW (2011) Gi-coupled gamma-aminobutyric acid-B receptors cross-regulate phospholipase C and calcium in airway smooth muscle. Am J Respir Cell Mol Biol 45:1232–1238.

Morland C, Andersson KA, Haugen ØP, Hadzic A, Kleppa L, Gille A, Rinholm JE, Palibrk V, Diget EH, Kennedy LH, Stølen T, Hennestad E, Moldestad O, Cai Y, Puchades M, Offermanns S, Vervaeke K, Bjørås M, Wisløff U, Storm-Mathisen J, et al (2017) Exercise induces cerebral VEGF and angiogenesis via the lactate receptor HCAR1. Nat Commun 8:15557.

Nikolaev VO, Bünemann M, Hein L, Hannawacker A, Lohse MJ (2004) Novel single chain cAMP sensors for receptor-induced signal propagation. J Biol Chem 279:37215–37218.

Offermanns S (2017) Hydroxy-carboxylic acid receptor actions in metabolism. Trends Endocrinol Metab 28:227–236.

Pellerin L, Magistretti PJ (1994) Glutamate uptake into astrocytes stimulates aerobic glycolysis: a mechanism coupling neuronal activity to glucose utilization. Proc Natl Acad Sci U S A 91:10625–10629.

Rhee SG (2001) Regulation of phosphoinositide-specific phospholipase C. Annu Rev Biochem 70:281–312.

Seino S, Shibasaki T (2005) PKA-dependent and PKA-independent pathways for cAMP-regulated exocytosis. Physiol Rev 85:1303–1342.

Serpa A, Ribeiro JA, Sebastião AM (2009) Cannabinoid CB(1) and adenosine A(1) receptors independently inhibit hippocampal synaptic transmission. Eur J Pharmacol 623:41–46.

Shimizu H, Watanabe E, Hiyama TY, Nagakura A, Fujikawa A, Okado H, Yanagawa Y, Obata K, Noda M (2007) Glial nax channels control lactate signaling to neurons for brain [Na^+] sensing. Neuron 54:59–72.

Sotelo-Hitschfeld T, Niemeyer MI, Mächler P, Ruminot I, Lerchundi R, Wyss MT, Stobart J, Fernández-Moncada I, Valdebenito R, Garrido-Gerter P, Contreras-Baeza Y, Schneider BL, Aebischer P, Lengacher S, San Martín A, Le Douce J, Bonvento G, Magistretti PJ, Sepúlveda FV, Weber B, et al (2015) Channel-mediated lactate release by K(+)-stimulated astrocytes. J Neurosci 35:4168–4178.

Suzuki A, Stern SA, Bozdagi O, Huntley GW, Walker RH, Magistretti PJ, Alberini CM (2011) Astrocyte-neuron lactate transport is required for long-term memory formation. Cell 144:810–823.

Tang F, Lane S, Korsak A, Paton JF, Gourine AV, Kasparov S, Teschemacher AG (2014) Lactate-mediated glia-neuronal signalling in the mammalian brain. Nat Commun 5:3284.

Tomura H, Itoh H, Sho K, Sato K, Nagao M, Ui M, Kondo Y, Okajima F (1997) Betagamma subunits of pertussis toxin-sensitive G proteins mediate A1 adenosine receptor agonist-induced activation of phospholipase C in collaboration with thyrotropin. A novel stimulatory mechanism through the cross talk of two types of receptors. J Biol Chem 272:23130–23137.

Wallenius K, Thalén P, Björkman JA, Johannesson P, Wiseman J, Böttcher G, Fjellström O, Oakes ND (2017) Involvement of the metabolic sensor GPR81 in cardiovascular control. JCI Insight 2:92564.

Wang M, Ramos BP, Paspalas CD, Shu Y, Simen A, Duque A, Vijayraghavan S, Brennan A, Dudley A, Nou E, Mazer JA, McCormick DA, Arnsten AF (2007) Alpha2A-adrenoceptors strengthen working memory networks by inhibiting cAMP-HCN channel signaling in prefrontal cortex. Cell 129:397–410.

Werry TD, Wilkinson GF, Willars GB (2003) Mechanisms of cross-talk between G-protein-coupled receptors resulting in enhanced release of intracellular Ca^{2+}. Biochem J 374:281–296.

Yang J, Ruchti E, Petit JM, Jourdain P, Grenningloh G, Allaman I, Magistretti PJ (2014) Lactate promotes plasticity gene expression by potentiating NMDA signaling in neurons. Proc Natl Acad Sci U S A 111:12228–12233.

Zhang C, Schmidt JT (1999) Adenosine A1 and class II metabotropic glutamate receptors mediate shared presynaptic inhibition of retinotectal transmission. J Neurophysiol 82:2947–2955.

Zhang Y, Chen K, Sloan SA, Bennett ML, Scholze AR, O'Keeffe S, Phatnani HP, Guarnieri P, Caneda C, Ruderisch N, Deng S, Liddelow SA, Zhang C, Daneman R, Maniatis T, Barres BA, Wu JQ (2014) An RNA-sequencing transcriptome and splicing database of glia, neurons, and vascular cells of the cerebral cortex. J Neurosci 34:11929–11947.